



ChemComm

Role of Acid Mixtures Etching on the Surface Chemistry and Sodium Ion Storage in $Ti_3C_2T_x$ MXene

Journal:	<i>ChemComm</i>
Manuscript ID	CC-COM-02-2020-001042.R1
Article Type:	Communication

SCHOLARONE™
Manuscripts

COMMUNICATION

Role of Acid Mixtures Etching on the Surface Chemistry and Sodium Ion Storage in $Ti_3C_2T_x$ MXene

Received 00th January 20xx,
Accepted 00th January 20xx

Mark Anayee^{ax}, Narendra Kurra^{ax}, Mohamed Alhabeab^a, Mykola Seredych^a, Mohamed Nejib Hedhili^c, Abdul-Hamid Emwas^c, Husam N. Alshareef^b, Babak Anasori^a, and Yury Gogotsi^{†a}

DOI: 10.1039/x0xx00000x

Two-dimensional transition metal carbides and/or nitrides (MXenes) have shown promise in developing electrochemical storage of metal ions within conductive galleries due to redox reactions with transition metal atoms. Here, effect of surface chemistry on electrochemical storage of sodium ions in MXene interlayer is investigated by etching Ti_3AlC_2 MAX using different etchants – HF, HF/HCl, and HF/ H_2SO_4 .

MXenes, a large family of layered materials comprised of transition metal carbides, nitrides, and carbonitrides, have become attractive candidates for a plethora of applications due to their compositional versatility and rich surface chemistry, leading to diverse physicochemical properties.¹ MXenes are synthesized through top-down wet chemical etching of MAX phases ($M_{n+1}AX_n$; M is an early transition metal such as Ti, V, Nb, Cr, Mo and A is Al, Ga, In, and X is C and/or N), where interleaved 'A' atomic layers are selectively extracted by fluoride containing etchants and replaced with surface functional groups ($-F$, $=O$, $-OH$, $-Cl$).² MXenes are hydrophilic yet the majority exhibit metallic conductivity and are generally represented by the formula $M_{n+1}X_nT_x$, where 'MX' lamellas are the same as in the MAX phase, and T_x refers to the surface functional groups. Colloidal suspensions of MXenes can be obtained through delamination of multilayered MXene lamellas by organic solvents, and inorganic and organic cations.³ Therefore, etching conditions, type of intercalant and the process of delamination have a strong impact on the optical, electronic, and physico-chemical properties of MXenes.⁴ Titanium carbide MXene ($Ti_3C_2T_x$) is the most widely studied member in the MXene

family and was the first MXene discovered. It has well-developed etching and delamination protocols, and it exhibits good chemical stability in dispersion and solid forms.⁴ Furthermore, $Ti_3C_2T_x$ exhibits unique properties such as record values of electrical conductivity exceeding 10,000 S/cm (free-standing films delaminated by lithium ions), a key parameter for a wide range of applications including electromagnetic interference shielding, electronics, wireless communication, and high-rate energy storage.⁵

There have been a few studies on the effect of etching conditions on the surface chemistry of MXenes. For example, Hope *et al.* investigated the surface of $Ti_3C_2T_x$ produced by HF and LiF/HCl methods using nuclear magnetic resonance (NMR) technique to confirm the coordination of $-F$ and $-OH$ as surface termination groups.⁶ Moreover, Sang *et al.* reported that the milder LiF/HCl etchant produces higher quality MXenes with lower concentration of point defects compared to 50 wt.% HF.⁷ Therefore, etchants with low concentration of HF (<10 wt%) are being used for $Ti_3C_2T_x$ synthesis due to recent demand for high quality MXenes for electronic and optoelectronic applications. However, there has been no systematic study on the nature of MXenes produced using low concentration of HF or using different anions in solution during the etching process. Our group previously reported that $Ti_3C_2T_x$ produced using HF/ H_2SO_4 showed better electrochemical energy storage of Na-ions compared to $Ti_3C_2T_x$ produced using HF and HF/HCl; however, no surface chemistry characterization was reported.⁸ Similarly, the aforementioned etching recipes for synthesis and processing of $Ti_3C_2T_x$ were previously demonstrated separately, but not compared directly using the same HF concentration.^{4, 9} Therefore, it is important to understand the surface chemistry state and analyze the remaining etching products in order to better control the factors that govern the chemical and electrochemical properties of MXenes.

In this study, we used HF and different acid mixtures, HF/HCl and HF/ H_2SO_4 – where the concentration of HF was 5 wt.% in all cases – to etch Ti_3AlC_2 MAX phase (Fig. 1a). In order to exclude the effect of Li-ions pre-intercalation, produced during in-situ etching methods employing LiF/HCl into the

^a A. J. Drexel Nanomaterials Institute, and Department of Materials Science and Engineering, Drexel University, Philadelphia, PA 19104, USA.

^b Materials Science and Engineering, Physical Science & Engineering Division, King Abdullah University of Science and Technology (KAUST), Thuwal, 23955-6900, Saudi Arabia.

^c Core Labs, King Abdullah University of Science and Technology (KAUST), Thuwal, 23955-6900, Saudi Arabia.

[†] Corresponding authors.

x These authors contributed equally to this work.

Electronic Supplementary Information (ESI) available: Experimental details, XRD, 4-point probe, XPS, ¹⁹F NMR, and TA-MS analysis. See DOI: 10.1039/x0xx00000x

multilayered MXene structure, this method was not investigated. The materials were also investigated at the multilayer stage in order to avoid any variations from the delamination process.⁴

X-ray diffraction (Fig. 1b) provides insight into the structural transformation of parent Ti_3AlC_2 MAX to $\text{Ti}_3\text{C}_2\text{T}_x$ MXenes. The (002) index is indicative of stacking order and interlayer spacing between $\text{Ti}_3\text{C}_2\text{T}_x$ layers. The (002) peak shifts from $2\theta = 9.5^\circ$ in Ti_3AlC_2 (Fig. S1a, Electronic Supplementary Information) to lower $2\theta = 9.1^\circ$ in $\text{Ti}_3\text{C}_2\text{T}_x$ (HF) (Fig. 1b), indicating that the interlayer spacing expands from 9.3 to 9.7 Å. Similarly, $\text{Ti}_3\text{C}_2\text{T}_x$ (HF/HCl) and $\text{Ti}_3\text{C}_2\text{T}_x$ (HF/ H_2SO_4) samples have (002) peaks shifted to lower 2θ values of 8.5° and 9.2° , corresponding to interlayer spacing values of 10.2 and 9.4 Å, respectively. The larger interlayer spacing values for $\text{Ti}_3\text{C}_2\text{T}_x$ samples with respect to Ti_3AlC_2 suggest that a minimal concentration of HF (5 wt.%) with/without the presence of other inorganic acids can accomplish the etching process with subsequent attachment of functional groups, T_x (-OH, =O, -F, -Cl), as shown previously.⁹ The subtle differences in the interlayer spacing of $\text{Ti}_3\text{C}_2\text{T}_x$ samples can be attributed to differences in the surface terminations and etching products, which can cause local variations in the interlayer spacing of MXene sheets.

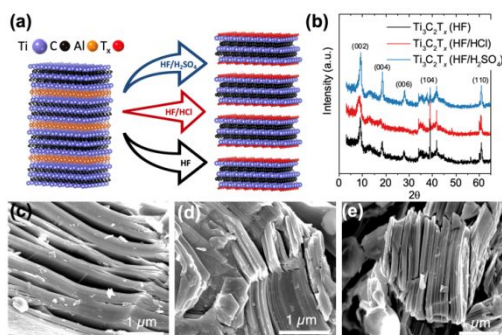


Fig. 1 Schematic illustrating the synthesis of $\text{Ti}_3\text{C}_2\text{T}_x$ MXene from the parent MAX phase by employing either HF, HF/HCl or HF/ H_2SO_4 etchants at a temperature of 40°C for 15 h (a). The corresponding XRD patterns (b) and SEM images of multilayered $\text{Ti}_3\text{C}_2\text{T}_x$ (HF) (c), $\text{Ti}_3\text{C}_2\text{T}_x$ (HF/HCl) (d) and $\text{Ti}_3\text{C}_2\text{T}_x$ (HF/ H_2SO_4) (e). HF concentration was 5 wt.% in all three cases.

The (002) peak appears broader and the intensity of the higher ordered (00l) indices such as the (004) peak appear weaker in $\text{Ti}_3\text{C}_2\text{T}_x$ (HF/HCl) compared to $\text{Ti}_3\text{C}_2\text{T}_x$ (HF) and $\text{Ti}_3\text{C}_2\text{T}_x$ (HF/ H_2SO_4) samples which suggests higher amount of structural water molecules (water strongly bonded to surface terminations) between the layers. While the water molecules were not enough to increase the interlayer spacing, however, they caused less ordered stacking along the *c*-lattice direction. It was also observed from the XRD patterns that there is a signature of residual MAX phase in the multilayered $\text{Ti}_3\text{C}_2\text{T}_x$ powders based on the (104) index, which is commonly present when etching with low concentrations of HF.⁴ Since only 5 wt.% HF was used, multilayered $\text{Ti}_3\text{C}_2\text{T}_x$ MXene is seen with thicker lamellas with fewer openings between interlayers at the microscale, as shown in Figs. 1c-e, compared to etching with higher concentrations of HF as shown by Alhabej *et al.*⁴

Also, since neither sonication nor delamination was done in this case, the morphology of MXene stacks observed was more compact. Overall, this indicates that morphology of the MXene layers is dependent on the concentration and type of etchant used for etching MAX.

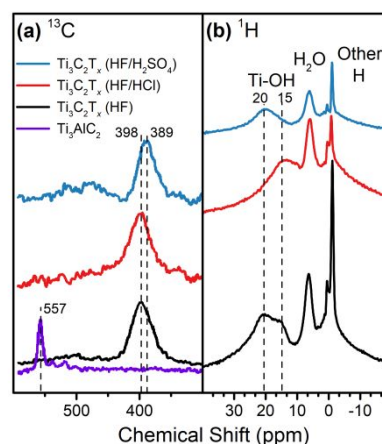


Fig. 2 ^{13}C NMR (a), and ^1H NMR (b) spectra of $\text{Ti}_3\text{C}_2\text{T}_x$ (HF), $\text{Ti}_3\text{C}_2\text{T}_x$ (HF/HCl) and $\text{Ti}_3\text{C}_2\text{T}_x$ (HF/ H_2SO_4) samples.

Solid-state NMR was used to probe the coordination of MXene core, surface terminations, and intercalants. ^{13}C NMR spectra (Fig. 2a) shows that precursor Ti_3AlC_2 was converted to $\text{Ti}_3\text{C}_2\text{T}_x$ as indicated by the shift in the peak from ~ 565 ppm to ~ 400 ppm, which is in agreement with previously reported chemical-shifts for $\text{Ti}_3\text{C}_2\text{T}_x$.^{6, 10} The disappearance of the Ti_3AlC_2 peak also points to complete or partial etching of all Ti_3AlC_2 , further confirming with the XRD (Fig. 2a) results, that 5 wt% HF with/without the presence of anions is enough to etch the Al layers. However, minute differences exist in the ^{13}C NMR spectra for the different samples, where the resonant peak for $\text{Ti}_3\text{C}_2\text{T}_x$ (HF) and (HF/HCl) is found at ~ 398 ppm, while for $\text{Ti}_3\text{C}_2\text{T}_x$ (HF/ H_2SO_4) it is found at ~ 389 ppm. These differences could stem from more electronegative species on the surface, such as hydrofluorocarbons in $\text{Ti}_3\text{C}_2\text{T}_x$ (HF), and higher amount of -O and -Cl terminations in $\text{Ti}_3\text{C}_2\text{T}_x$ (HF/HCl), which lead to a more diffuse overlap of Ti 3d with C 2p orbitals. This difference in the electron densities around the Ti and C leads to a more de-shielded ^{13}C nucleus and thus a larger chemical shift. Moreover, the resonance peak for the $\text{Ti}_3\text{C}_2\text{T}_x$ (HF/HCl) sample appears broader than that of the other samples, which suggests a longer T_2 relaxation time, and thus a higher electron density on Ti atoms. However, this is contrary to the four-point probe measurements where $\text{Ti}_3\text{C}_2\text{T}_x$ (HF/ H_2SO_4) was found to exhibit the highest conductivity (Fig. S1b, ESI). Thus, further studies are needed to understand the differences, which may stem from other factors such as presence of Ti vacancies or lack thereof.⁷

^1H NMR spectra (Fig. 2b) showed a broad peak around 15-20 ppm assigned to Ti-OH surface terminations, an intermediate peak ~ 7 ppm assigned to intercalated water, and a sharp peak ~ 0 ppm assigned to intercalated contaminants.^{6, 10a} The following discussion highlights the advantages of using

^1H NMR spectra to distinguish between H_2O and OH signals compared to other characterization techniques.

Interestingly, the Ti-OH peak is broader for $\text{Ti}_3\text{C}_2\text{T}_x$ (HF) compared to $\text{Ti}_3\text{C}_2\text{T}_x$ (HF/HCl) and $\text{Ti}_3\text{C}_2\text{T}_x$ (HF/ H_2SO_4). The differences are attributed to variations in the local environment, i.e., the type and amount of neighbouring surface terminations. For example, it is possible that $-\text{Cl}$ surface terminations on the $\text{Ti}_3\text{C}_2\text{T}_x$ (HF/HCl) sample could be responsible for a chemical shift of -5 ppm for Ti-OH signals (XPS data, Fig. S2, ESI). On the other hand, the $-\text{OH}$ surface terminations might be due to two different sites or interactions on the surface as indicated by the two dashed lines in Fig. 2b. The $\text{Ti}_3\text{C}_2\text{T}_x$ (HF) sample exhibits both sites based on the peaks at 15 ppm and 21 ppm, while the $\text{Ti}_3\text{C}_2\text{T}_x$ (HF/HCl) sample exhibits only the first site based on the peak at 14 ppm. In the case of the $\text{Ti}_3\text{C}_2\text{T}_x$ (HF/ H_2SO_4) sample, the peak at 20 ppm suggests the material only has the second site. This follows Persson *et al.*, where it was proposed that O 1s XPS spectra for $\text{Ti}_3\text{C}_2\text{T}_x$ can be deconvoluted into two contributions from oxygen surface terminations in the A site, with and without interactions from nearby fluoride surface terminations.¹¹

Furthermore, the relative ratio of H_2O signal to Ti-OH signal can be used as a measure of the amount of structural water in the samples, which was found to be higher for $\text{Ti}_3\text{C}_2\text{T}_x$ (HF/HCl) compared to other etching methods (Fig. 2b). Moreover, higher amount of water in $\text{Ti}_3\text{C}_2\text{T}_x$ (HF/HCl) was also confirmed by a broader (002) peak in XRD (Fig. 1b) and thermogravimetric analysis coupled with mass spectrometry data (Fig. S3-S4, ESI).

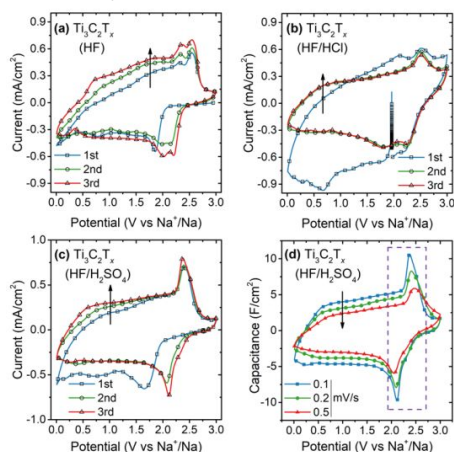


Fig. 3 Na-ion half-cells using $\text{Ti}_3\text{C}_2\text{T}_x$ MXene pellet electrodes. Cyclic voltammograms showing first three cycles at a scan rate of 0.1 mV/s using working electrodes of $\text{Ti}_3\text{C}_2\text{T}_x$ (HF) (a), $\text{Ti}_3\text{C}_2\text{T}_x$ (HF/HCl) (b) and $\text{Ti}_3\text{C}_2\text{T}_x$ (HF/ H_2SO_4) (c). CVs of $\text{Ti}_3\text{C}_2\text{T}_x$ (HF/ H_2SO_4) at different scan rates (d).

To investigate the intrinsic electrochemical Na-ion intercalation and storage in $\text{Ti}_3\text{C}_2\text{T}_x$, Na-ion half-cells were assembled. Multilayered $\text{Ti}_3\text{C}_2\text{T}_x$ powders were cold pressed into disc electrodes with thickness ~ 270 μm and density ~ 2.8 g/cm^3 (for 100 mg powder). Density of $\text{Ti}_3\text{C}_2\text{T}_x$ pellets was about three times higher compared to conventional slurry casting method ($0.8\text{--}1$ g/cm^3). Thus, obtained $\text{Ti}_3\text{C}_2\text{T}_x$ discs were binder and conductive additive-free and were directly

used as working electrodes in assembling Na-ion half cells with Na-foil as counter and reference electrodes in non-aqueous Na^+ electrolyte. As shown in Fig. 3, CV scans for the first three cycles are displayed at a scan rate of 0.1 mV/s in the potential range of 0.01 - 3 V (vs. Na^+/Na). The first cycle Coulombic Efficiency values were found to be 64%, 53% and 60% for the $\text{Ti}_3\text{C}_2\text{T}_x$ HF, HF/HCl, and HF/ H_2SO_4 etched electrodes, respectively. First cycle irreversibility differences could be attributed to the different surface terminations and amounts of structural water in those samples.¹² For example, Kurahashi *et al.* reported that fluoride and oxygen surface terminations are favorable for sodium ion adsorption in opposition to hydroxyl surface terminations.¹³ The electrochemical results corroborate very well with the XPS, NMR and mass spectrometry data.

Interestingly, $\text{Ti}_3\text{C}_2\text{T}_x$ MXene electrodes showed redox peaks above 2V (vs. Na^+/Na), which can be attributed to the redox reaction of the $\text{Ti}^{+3}/\text{Ti}^{+2}$ couple.^{14a} Traditionally, titanium-based electrodes benefit from the redox reaction of $\text{Ti}^{+3}/\text{Ti}^{+2}$ to insert Na-ions.¹⁴ Therefore, the intrinsic redox nature of $\text{Ti}_3\text{C}_2\text{T}_x$ might be preserved by employing mild concentration of fluoride solutions during the etching process. For instance, as can be seen from Fig. 3a, $\text{Ti}_3\text{C}_2\text{T}_x$ (HF) showed two pairs of redox peaks (oxidation/reduction at 2.37 V/2.02 V and 2.55 V/2.21 V vs. (Na^+/Na)) while $\text{Ti}_3\text{C}_2\text{T}_x$ (HF/HCl) and $\text{Ti}_3\text{C}_2\text{T}_x$ (HF/ H_2SO_4) electrodes showed a single pair of redox peaks positioned at 2.52 V/2.25 V and 2.41 V/2.12 V, respectively (Figs. 3b, 3c). These experiments suggest that the titanium surface state and oxidation differ in each case as suggested by the positions of redox peaks. However, the prominent appearance of redox peaks in all three cases is an indication for the intrinsic redox behavior of $\text{Ti}_3\text{C}_2\text{T}_x$. Similarly, Dall'agnese *et al.* also observed prominent redox peaks for V_2CT_x electrodes in non-aqueous Na^+ electrolyte.¹⁵ Therefore, metal surfaces such as Ti and V can show redox nature in non-aqueous electrolytes as well.¹⁶ This could be due to ion insertion induced redox reaction of the metal atoms of MXene, by maintaining charge neutrality.¹⁷

Compared to HF and HF/HCl, HF/ H_2SO_4 etched sample showed close to rectangular CV shape below 2 V and more pronounced redox peaks above 2 V (vs. Na^+/Na). This might be due to the clean surface of MXene electrodes, as H_2SO_4 can dissolve and remove the etching by-products as indicated by ^{19}F NMR results (Fig. S5, ESI), and also superior conductivity over other samples – 96, 110, and 714 S/cm for HF, HF/HCl, and HF/ H_2SO_4 etched samples pressed into disc electrodes, respectively. Further, $\text{Ti}_3\text{C}_2\text{T}_x$ (HF/ H_2SO_4) pellets were swept at different scan rates and showed prominent redox peaks (Fig. 3d). Anodic and cathodic peak current responses vary linearly with the scan rate (0.1–0.5 mV/s), suggesting that surface controlled redox reactions occur.

After the initial Na^+ intercalation, $\text{Ti}_3\text{C}_2\text{T}_x$ electrodes exhibit pseudocapacitive behavior and stable rectangular CV below 2 V (Vs. Na^+/Na), corresponding to typical capacitor behavior, at such high mass-loading of 75 mg/cm^2 (commercial scale mass-loading is ~ 10 mg/cm^2), and gravimetric capacity of 44 mAh/g at 0.1 mV/s (corresponding to volumetric capacity of 124

mAh/cm³). Typical areal capacities vary from 3.3 to 2.1 mAh/cm² in the scan rate of 0.1 to 0.5 mV/s. Kim *et al.* also reported stable lithiation capacities up to 5 mAh/cm² for Ti₃C₂T_x electrodes at a similarly high mass-loading of 50 mg/cm².¹⁸ As this study mainly focuses on determining the influence of etching conditions on the surface chemistry and the intrinsic electrochemical properties, the electrochemical performance and its optimization should be the focus of further studies.

In summary, systematic investigation of etching Ti₃AlC₂ MAX using three different etchants – HF, HF/HCl, and HF/H₂SO₄ – led to Ti₃C₂T_x MXenes with diverse surface terminations (=O, -OH, -F, and -Cl) and different amounts of structural water. HF/HCl etching produced -Cl terminations, which might be the cause for the observed larger interlayer spacing and larger amount of structural water compared to HF and HF/H₂SO₄ etched samples. Etching with HF/H₂SO₄ led to only a trace sulfur signal and the highest electrical conductivity and thermal stability values compared to the other etching methods. Furthermore, ¹H NMR revealed variations in the Ti-OH peaks for the different samples, which could be attributed to multiple adsorption sites for -OH surface terminations; with and without interaction of nearby fluoride. Investigation of electrochemical sodium ion intercalation revealed that Ti₃C₂T_x (HF/H₂SO₄) sample had lower first cycle irreversibility and better overall electrochemical performance, which may be attributed to a cleaner surface due to better removal of etching by-products and structural water.

Since the three etching methods were shown to influence the surface chemistry and physicochemical properties of MXene, this work highlights the need to further investigate their impact on physicochemical properties, as well as performance of MXenes in various applications aside from Na-ion storage, such as electromagnetic interference shielding or antennas, which rely heavily on the electrical conductivity of the material.

Acknowledgments: Collaboration between King Abdullah University of Science and Technology (KAUST) and Drexel University was supported by KAUST-Drexel Competitive Research Grant (URF/1/ 2963-01-01). M. Anayee was supported by the National Science Foundation Graduate Research Fellowship under Grant #DGE-1646737. Any opinion, findings, and conclusion or recommendations expressed in this material are those of the author(s) and do not necessarily reflect the views of the National Science Foundation. SEM and XRD were performed at the Drexel University Core Research Facilities (CRF). Authors thank Kathleen Maleski (Drexel University) for invaluable comments and discussions and the Advanced Nanofabrication, Imaging and Characterization Laboratory at KAUST for experimental support.

Conflicts of interest

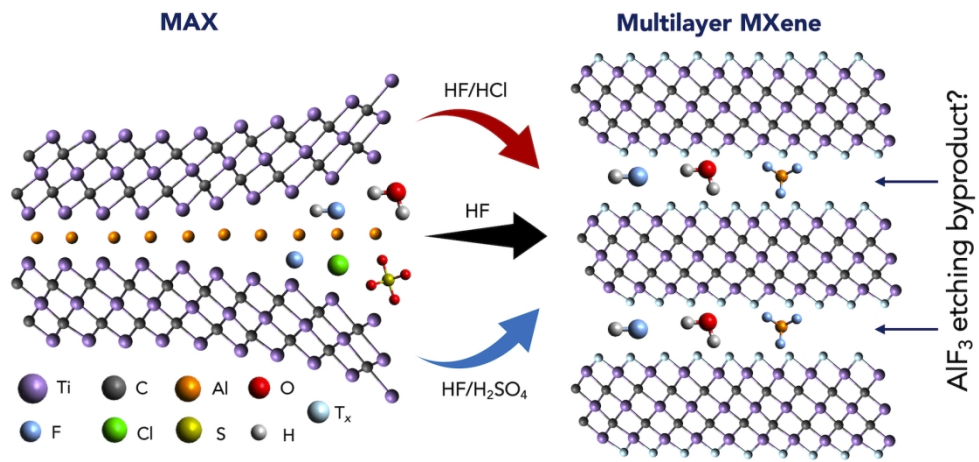
There are no conflicts to declare

References

1. B. Anasori and Y. Gogotsi, *2D Metal Carbides and Nitrides (MXenes): Structure, Properties and Applications*, Springer, 2019.
2. Y. Gogotsi and B. Anasori, *ACS Nano*, 2019, **13**, 8491.
3. (a) O. Mashtalir, M. Naguib, V. N. Mochalin, Y. Dall'Agnese, M. Heon, M. W. Barsoum and Y. Gogotsi, *Nat. Commun.*, 2013, **4**, 7; (b) M. Ghidui, M. R. Lukatskaya, M. Q. Zhao, Y. Gogotsi and M. W. Barsoum, *Nature*, 2014, **516**, 78; (c) M. Naguib, R. R. Unocic, B. L. Armstrong and J. Nanda, *Dalton Trans.*, 2015, **44**, 9353.
4. M. Alhabeab, K. Maleski, B. Anasori, P. Lelyukh, L. Clark, S. Sin and Y. Gogotsi, *Chem. Mat.*, 2017, **29**, 7633.
5. (a) F. Shahzad, M. Alhabeab, C. B. Hatter, B. Anasori, S. M. Hong, C. M. Koo and Y. Gogotsi, *Science*, 2016, **353**, 1137; (b) Z. W. Wang, H. Kim and H. N. Alshareef, *Adv. Mater.*, 2018, **30**, 7; (c) A. Sarycheva, A. Polemi, Y. L. Liu, K. Dandekar, B. Anasori and Y. Gogotsi, *Sci. Adv.*, 2018, **4**, 8; (d) Q. Jiang, N. Kurra, K. Maleski, Y. J. Lei, H. F. Liang, Y. Z. Zhang, Y. Gogotsi and H. N. Alshareef, *Adv. Energy Mater.*, 2019, **9**, 1901061; (e) Y. Y. Peng, B. Akuzum, N. Kurra, M. Q. Zhao, M. Alhabeab, B. Anasori, E. C. Kumbur, H. N. Alshareef, M. D. Ger and Y. Gogotsi, *Energy Environ. Sci.*, 2016, **9**, 2847.
6. M. A. Hope, A. C. Forse, K. J. Griffith, M. R. Lukatskaya, M. Ghidui, Y. Gogotsi and C. P. Grey, *Phys. Chem. Chem. Phys.*, 2016, **18**, 5099.
7. X. H. Sang, Y. Xie, M. W. Lin, M. Alhabeab, K. L. Van Aken, Y. Gogotsi, P. R. C. Kent, K. Xiao and R. R. Unocic, *ACS Nano*, 2016, **10**, 9193.
8. N. Kurra, M. Alhabeab, K. Maleski, C. H. Wang, H. N. Alshareef and Y. Gogotsi, *ACS Energy Lett.*, 2018, **3**, 2094-2100.
9. C. A. Voigt, M. Ghidui, V. Natu and M. W. Barsoum, *J. Phys. Chem. C*, 2018, **122**, 23172.
10. (a) K. J. Harris, M. Bugnet, M. Naguib, M. W. Barsoum and G. R. Goward, *J. Phys. Chem. C*, 2015, **119**, 13713; (b) K. J. D. Mackenzie, R. H. Meinhold, D. G. McGavin, J. A. Ripmeester and I. Moudrakovski, *Solid State Nucl. Magn. Reson.*, 1995, **4**, 193.
11. I. Persson, L. A. Naslund, J. Halim, M. W. Barsoum, V. Darakchieva, J. Palisaitis, J. Rosen and P. O. A. Persson, *2D Mater.*, 2017, **5**, 015002.
12. X. Guo, W. Zhang, J. Zhang, D. Zhou, X. Tang, X. Xu, B. Li, H. Liu and G. Wang, *ACS Nano*, 2020, **14**, 3651.
13. S. Kurahashi, S. Arabnejad, H. Ushiyama and K. Yamashita, *J. Comput. Chem.-Jpn.*, 2019, **18**, 84.
14. (a) M. Okubo, A. Sugahara, S. Kajiyama and A. Yamada, *Accounts Chem. Res.*, 2018, **51**, 591; (b) J. Yin, L. Qi and H. Y. Wang, *ACS Appl. Mater. Interfaces*, 2012, **4**, 2762; (c) S. H. Guo, J. Yi, Y. Sun and H. S. Zhou, *Energy Environ. Sci.*, 2016, **9**, 2978; (d) J. Nan, X. Guo, J. Xiao, X. Li, W. Chen, W. Wu, H. Liu, Y. Wang, M. Wu and G. Wang, *Small*, 2019, 1902085
15. Y. Dall'Agnese, M. R. Lukatskaya, K. M. Cook, P. L. Taberna, Y. Gogotsi and P. Simon, *Electrochem. Commun.*, 2014, **48**, 118.
16. (a) X. Q. Xie, M. Q. Zhao, B. Anasori, K. Maleski, C. E. Ren, J. W. Li, B. W. Byles, E. Pomerantseva, G. X. Wang and Y. Gogotsi, *Nano Energy*, 2016, **26**, 513; (b) Y. Xie, Y. Dall'Agnese, M. Naguib, Y. Gogotsi, M. W. Barsoum, H. L. L. Zhuang and P. R. C. Kent, *ACS Nano*, 2014, **8**, 9606. (c) X. Wang, S. Kajiyama, H. Iinuma, E. Hosono, S. Oro, I. Moriguchi, M. Okubo and A. Yamada, *Nat. Commun.*, 2015, **6**, 6544.
17. (a) S. Kajiyama, L. Szabova, K. Sodeyama, H. Iinuma, R. Morita, K. Gotoh, Y. Tateyama, M. Okubo and A. Yamada, *ACS Nano*, 2016, **10**, 3334; (b) A. VahidMohammadi, A. Hadjikhani, S. Shahbazmohammadi and M. Beidaghi, *ACS Nano*, 2017, **11**, 11135.
18. S. J. Kim, M. Naguib, M. Q. Zhao, C. F. Zhang, H. T. Jung, M. W. Barsoum and Y. Gogotsi, *Electrochim. Acta*, 2015, **163**, 246.

The following is the caption to accompany the table of contents entry graphic:

Optimizing the etchants for MXene synthesis to remove etching byproducts, obtain pristine surface chemistry, and improve energy storage performance.



79x39mm (600 x 600 DPI)